PAPER

Cu-releasing bioactive glass/polycaprolactone coating on Mg with antibacterial and anticorrosive properties for bone tissue engineering

Biomedical Materials

PAPER

Cu-releasing bioactive glass/polycaprolactone coating on Mg with antibacterial and anticorrosive properties for bone tissue engineering

RECEIVED
5 May 2017

REVISED
17 July 2017

ACCEPTED FOR PUBLICATION
23 August 2017

PUBLISHED
26 October 2017

Yuyun Yang[1,2], Kai Zheng[1], Ruifang Liang[3], Astrid Mainka[4], Nicola Taccardi[5], Judith A Roether[6], Rainer Detsch[1], Wolfgang H Goldmann[4], Sannakaisa Virtanen[2,7] and Aldo R Boccaccini[1,7]

[1] Institute of Biomaterials, Department of Materials Science and Engineering, University of Erlangen-Nuremberg, Erlangen, Germany
[2] Institute for Surface Science and Corrosion, Department of Materials Science and Engineering, University of Erlangen-Nuremberg, Erlangen, Germany
[3] Department of Internal Medicine 3 and Institute for Clinical Immunology, University Clinics, Erlangen, Germany
[4] Biophysics Group, Department of Physics, University of Erlangen-Nuremberg, Erlangen, Germany
[5] Institute of Chemical Reaction Engineering, University of Erlangen-Nuremberg, Erlangen, Germany
[6] Institute of Polymer Materials, Department of Materials Science and Engineering, University of Erlangen-Nuremberg, Erlangen, Germany
[7] Authors to whom any correspondence should be addressed.

E-mail: virtanen@ww.uni-erlangen.de **and** aldo.boccaccini@ww.uni-erlangen.de

Keywords: magnesium, bioactive glass, PCL, antibacterial activity, anticorrosion

Abstract

Bioactive glass nanoparticles containing copper (Cu-BGNs) were introduced into polycaprolactone (PCL) coating systems to improve the bioactivity, antibacterial properties, and corrosion resistance of vulnerable magnesium matrices under physiological conditions. The influence of different amounts of Cu-BGNs in PCL coatings was thoroughly investigated in determining the wettability, electrochemical properties, and antibacterial effects against *Staphylococcus carnosus* and *Escherichia coli,* as well as their cyto-compatibility. Cu-BGNs were observed randomly scattered in PCL coatings. Increasing the concentration of Cu-BGNs resulted in a slight decrease of the water contact angle, and a reduction in anticorrosion properties of the Cu-BGN composite coatings. Yet higher Cu-BGN content in coatings led to more calcium phosphate formation on the surface after 7 days of immersion in Dulbecco's modified Eagle's medium, which was confirmed by Fourier-transform infrared spectroscopy and x-ray photoelectron spectroscopy. The growth of *S. carnosus* and *E. coli* was inhibited by Cu^{2+} ions released from the Cu-BGN coatings. In addition, both direct and indirect cyto-compatibility experiments showed that the viability and proliferation of MG-63 cells on Cu-BGN coatings were highly increased compared to pure magnesium; however, an additional increase of Cu-BGN concentration showed a slight decrease of cell proliferation and cell activity. In summary, Cu-BGN/PCL composite coatings impart magnesium-based biomaterials with antibacterial and anticorrosive properties for clinical applications.

1. Introduction

Due to the attractive properties of magnesium and magnesium alloys, such as similar physical and mechanical properties (low density (1.738 g cm^{-3})), superior fracture toughness, and moderate elastic modulus (45 GPa), which is close to that of natural bone, there is increasing interest in their biomedical applications [1–3]. However, the high degradation rate of magnesium results in hydrogen evolution and subsequent unacceptable pH value changes, which lead to excessive inflammatory response and could result in the failure of the implant [4–6]. Therefore, clinical applications of magnesium are largely restricted. Many attempts have been made to increase the corrosion resistance and biological activity of magnesium in biological systems, for example by applying protective biodegradable coatings [7–12].

Bio-reabsorbable polymers have attracted increasing attention for biomedical applications. The traditional

polyesters poly lactic acid (PLA), poly glycolic acid (PGA), poly lactic acid-co-glycolic acid (PLGA), polycaprolactone (PCL), and their copolymers, have demonstrated promising results in clinical use [13]. Biodegradable polymer coating systems are being also employed to improve the corrosion resistance of magnesium [11, 14]. Furthermore, bioactive glasses (BGs) have been widely investigated *in vitro* and *in vivo* due to their outstanding osteo-conductivity and bioactivity, and their controllable biodegradability [15]. Various methods, such as melting, sol–gel and flame synthesis [15–17] are suitable for producing BGs. The introduction of different ions into BG compositions is an interesting approach to improve the angiogenic and antibacterial properties of BGs [18, 19]. In particular, the antibacterial effect could reduce the nosocomial infection rates on the medical devices.

In this study, biodegradable PCL incorporated with sol–gel derived copper-containing BG nanoparticles (Cu-BGNs) were used to produce composite coatings on magnesium substrates, which were generated by the spin coating method. Different amounts of Cu-BGNs were incorporated in PCL-based coatings on magnesium. The influence of the Cu-BGN addition on the corrosion protective ability of PCL coatings was investigated by electrochemical and short-term immersion tests in Dulbecco's modified Eagle's medium (DMEM). In addition, the antibacterial activity and cyto-compatibility of coated specimens were studied along with the release behavior of Cu^{2+} ions from PCL coatings. While BG-polymer composite coatings have already been investigated on Mg/Mg alloys [11], this is the first study that considers novel BG particles loaded with the biologically active element Cu.

2. Experimental

2.1. Preparation of materials

Pure magnesium (99.99% purity, Chempur Feinchemikalien und Forschungsbedarf GmbH) samples of 2–4 mm thickness and 24.5 mm diameter were prepared from commercially available magnesium rods. The samples were grounded, using 2000 grit SiC papers followed by fine polishing down to 0.25 microns. The samples were rinsed with ethanol in an ultrasonic bath for 2 min to remove any particles from the surface. Finally, samples were rinsed with ethanol and dried in hot air.

PCL (Sigma-Aldrich) with a molecular weight of 70 000–90 000 g mol^{-1} and Cu-BGNs were employed to prepare the coatings. BGNs were synthesized, using a modified Stöber method as reported in a previous study [20]. Spin coating on Mg samples was performed in a similar way as reported previously [11], solutions of 7.5 wt% PCL in chloroform were used for all coatings in this study. Different amounts of Cu-BGNs were added to the PCL solutions to prepare different coatings containing 1 wt% (1Cu-BGN), 2 wt% (2Cu-BGN) and 5 wt% (5Cu-BGN).

2.2. Physico-chemical characterization

The cross-section and topography of Cu-BGN composite coatings were observed using scanning electron microscopy (SEM, model Auriga, Zeiss). Au was sputtered on the surface of the samples to obtain conductive surfaces preventing charge effects during SEM imaging. The weight of coatings was calculated from weight differences of the samples before and after spin coating. The wettability of the composite coatings was measured by static water contact angles with a DSA30 instrument (Kruess GmbH). All data were collected from mean values of eight independent measurements. Fourier-transform infrared spectroscopy (FTIR, Nicolet 6700, Thermo Scientific) and x-ray photoelectron spectroscopy (XPS, PHI 5600) were used to characterize the chemical composition of the coatings.

2.3. Electrochemical measurements and immersion tests

Electrochemical behavior of samples was measured by an electrochemical workstation 'IM6eX' (Zahner-Elektrik GmbH & Co. KG, Kronach). The same 'three-electrode system' reported in previous studies was used for electrochemical tests [11]. In brief, the coated samples were used as the working electrode, a platinum plate as the auxiliary electrode, and an Ag/AgCl electrode in 3 M KCl as the reference electrode. Electrochemical impedance spectroscopy (EIS) and potentiodynamic polarization tests were performed in DMEM (Biochrome AG). Every experiment was repeated at least three times. The immersion tests were performed for 7 days in DMEM at 37 °C. The medium was refreshed after 3 days of immersion.

2.4. ICP-AES determination

Inductively coupled plasma atomic emission spectroscopy (ICP-AES) was used to determine the Cu^{2+} ion releasing behavior in DMEM. The amount of Cu^{2+} was detected by using its emission line at 324.754 nm and Si at 251.612 nm. The testing medium was diluted by distilled water when the concentration was too high. All experiments were conducted in triplicate.

2.5. Antibacterial tests

The antibacterial activity of Cu-BGN composite coatings was evaluated against gram-positive (*Staphylococcus carnosus*) and gram-negative (*Escherichia coli*) bacteria. The assessment was carried out quantitatively, using a 96-well turbi-dimetric procedure based on the light absorbance (optical density (OD)) caused by turbidity of bacterial growth in suspension [21, 22]. In brief, the bacterial strains were grown in nutrient broth, LB medium (Carl Roth GmbH, Karlsruhe),

according to the manufacturer's instructions at 37 °C, simultaneously shaking for 24 h to reach the logarithmic phase of growth. The bacterial suspensions were then diluted with LB medium by adjusting the OD_{600nm} value to 0.01 for further antibacterial use. Solution extracts were prepared for antibacterial tests, using immersion samples in sterilized phosphate-buffered saline (PBS) for 72 h at 37 °C in a shaker. The ratio of the surface area of the coatings to the volume of extraction medium was 1 cm^2 ml^{-1}. Individual wells of the 96-well microplate (Corning, Cambridge, MA) were incubated with 50 μl of bacterial suspension and 50 μl of extract solution. Reference wells contained 50 μl of bacterial suspension and 50 μl of PBS. 100 μl of PBS in wells was used as a background. The experiments were repeated six times. The OD of bacterial growth was recorded before and after 24 h of culture at 600 nm, using a microplate reader (PHOmo, autobiolabtec instruments co. Ltd, Zhengzhou). The OD value for each sample was calculated as follows:

$$OD_{600nm}\text{value}_{sample} = \text{OD value}_{before} - \text{OD value}_{after} - \text{OD value}_{background}$$

2.6. *In vitro* cyto-compatibility (direct and indirect methods)

The human osteosarcoma cell line (MG-63; Sigma-Aldrich) was used for *in vitro* cell biocompatibility assessment of Cu-BGN coatings. The cytotoxicity tests were carried out by direct and indirect contact methods. MG-63 cells were cultured in DMEM (Gibco) supplemented with 10 vol.% fetal bovine serum (FBS; Sigma-Aldrich) and 1 vol.% penicillin/streptomycin (Pen Strep; Sigma-Aldrich) and incubated at 37 °C in a humidified atmosphere of 5% CO_2. Cells were grown as a monolayer on 75 cm^2 canted-neck cell culture flasks (Greiner-Bio One) for 48 h to 80%–90% confluence. The old medium was discarded, and then cells were washed with PBS (Gibco). Thereafter, trypsin/EDTA (Life Technology) was used to detach cells from the flask wall. The number of live cells was counted in a hemocytometer by adding trypan blue (Sigma-Aldrich). Cell concentrations of 1×10^5 ml^{-1} were achieved by dilution with culture medium.

2.6.1. Direct cytotoxicity

MG-63 cells were seeded in 24-well plates containing sterilized samples for 72 h incubation in a humidified atmosphere at 5% CO_2 and 37 °C. The cell viability was quantified (WST-8 assay; Sigma-Aldrich) by assessing the mitochondrial activity in cells. Before adding 100 μl new DMEM containing 1 vol% WST-8 reagent in each well, the old culture medium was removed, and the cells were rinsed thoroughly with PBS. The absorbance was recorded at 450 nm on a microplate reader post 2 h of incubation at 37 °C. The absorbance of the positive control was considered as a 100% viability value and that of DMEM with 1 vol% WST-8 reagent was recorded as a blank. The relative cell viability was calculated as follows:

$$\text{Cell viability} = \frac{\text{OD(test)} - \text{OD(blank)}}{\text{OD(positive control)} - \text{OD(blank)}} \times 100\%$$

The cell morphology and distribution were studied by labeling with Vybrant®Dil cell tracers (Life Technologies, Darmstadt) according to the manufacturer's instructions. Briefly, the samples were washed with PBS and 1 ml master mix solution containing 4 μl Vybrant®Dil per 1 ml DMEM culture medium in the well. After 45 min of incubation, the cells were fixed in a fixing solution for 15 min. The bone mineralization assay was closely followed after the fixing steps. Mineralization assays were performed by using OsteoImage™ fluorescent staining kit (Lonza), which is based on the specific binding to the hydroxyapatite portion of bone-like nodules deposited by cells. The samples were washed twice with OsteoImage™ wash buffer (ten times diluted) after fixation. The diluted (1:100) OsteoImage™ staining reagent was used to stain cells and left to incubate for 30 min away from light. Then three washes with buffer were performed for 5 min each. The samples were kept in PBS and images were taken by a fluorescence microscope (FM).

Cell proliferation was determined through the total activity of lactate dehydrogenase (LDH) in the cell lysates using an LDH-activity quantification kit (TOX7, Sigma-Aldrich). Samples were washed with PBS and lysed with a buffer containing 10 mm Tris–HCl, 1 mM $MgCl_2$, and 0.05% Triton X-100 at pH 7.5 for 30 min at 37 °C in a shaker. After that, the surface of samples was scratched with pipette tips to remove all attached cells in the lysis buffer. The lysate solutions were centrifuged for 5 min at 2000 rpm, and 140 μl supernatant was transferred into a 1 ml cuvette. 60 μl of LDH master mix was added to each sample in the cuvette, and the incubation was processed at 37 °C for 30 min away from light. The enzymatic reaction was stopped by adding 300 μl HCl (1 M), and each cuvette was filled with 500 μl of distilled water. The dye was measured using a spectrophotometer (SPECORD 40 BU, Analytik, Jena) at 490 nm and 600 nm.

To characterize the osteoblast differentiation of MG-63 cells, alkaline phosphatase (ALP) activity was analyzed by measuring the specific enzyme activity after 72 h of incubation. The supernatant of the lysed cells was prepared by following the same procedure as for LDH. 250 μl supernatant was added to 100 μl alkaline buffer (pH 9.8) containing 9 mM p-nitrophenyl phosphate (pNPP), 0.1 mM Tris, and 2 mM $MgCl_2$; the mixture was then incubated at 37 °C. The reaction was stopped by adding 650 μl of 1 M NaOH solution, and the absorbance was measured in a UV–vis

spectrophotometer. The ALP activity was determined by measuring the optical density at 405 nm and 690 nm.

2.6.2. Cytotoxicity evaluation of extraction medium (indirect assay)

Extracts were prepared according to ISO 10993-5:1999 [23], and the ratio of surface area/extraction medium volume was 1 cm^2/5 ml. After 48 h of incubation in DMEM in a 6-well plate (Corning, Cambridge, MA) at a humidified atmosphere with 5% CO_2 at 37 °C, the extraction medium was collected for indirect assays. Culture medium (100 μl) with 1000 MG-63 cells was pre-seeded in each well of a 96-well plate and was incubated at a humidified atmosphere with 5% CO_2 at 37 °C for 24 h to allow for cell attachment. After that, the old medium was replaced with 100 μl extracts. The cell culture in the well containing 100 μl DMEM was taken as the positive control. Then the 96-well plate was incubated in a humidified atmosphere with 5% CO_2 at 37 °C for another 48 h. Afterwards, the cell activity was detected by WST-8 assay. Live-staining was performed with calcein acetoxymethyl ester (Calcein-AM, Invitrogen) after 48 h of cultivation. The old culture medium was discarded, and the samples were washed thoroughly with PBS. 1 ml master mix (5 μl Calcein-AM solution in 1 ml PBS) was added in each well and incubated for 45 min. After that, the mix solution was removed and washed with PBS again. A fixing solution containing 3.7% paraform-aldehyde in PBS was added to the samples for 15 min. Then the solution was discarded, and the samples were kept in PBS in the dark for further characterization. A FM (Axio Scope A.1, Carl Zeiss Microimaging GmbH) was used to take images of Calcein-AM-stained cells.

2.7. Statistical analysis

All quantitative data were collected from six replicates and were reported as mean values, ± standard deviation (SD). Statistical analysis of mitochondrial activity in cells was accomplished by using one-way analysis of variance (ANOVA) on the different coatings compared to pure magnesium samples after incubation. The paired two samples for mean values were performed by the Student–Newman–Keuls method. The value $p < 0.05$ was considered as statistically significant: $^{*}p < 0.05$, $^{**}p < 0.01$ and $^{***}p < 0.001$.

3. Results and discussion

3.1. Morphology and composition of coatings

The morphology of both the surface and the cross-section of the composite coatings, incorporated with different amounts of Cu-BGNs, was observed by SEM.

The surface morphology at different magnifications of 1Cu-BGN, 2Cu-BGN, and 5Cu-BGN coatings are displayed in figures 1(a1)–(a3), (b1)–(b3), and (c1)–(c3), respectively. As shown at low magnification in figures 1(a1), (b1), (c1), BG clusters are randomly distributed. A high content of Cu-BGNs incorporated in PCL caused increasing cluster formation. The smaller Cu-BGN clusters were completely covered by PCL, and the larger ones were partially buried in PCL, as shown in figures 1(a2), (b2), (c2). Besides the larger clusters, single Cu-BGN particles were distributed in the coating, as observed in figures 1(a3), (b3), (c3) at higher magnification. The grain boundary of semi-crystalized PCL is also more visible in the higher magnification images.

In order to examine the distribution of Cu-BGN in the composite coating, the cross-sections of pure PCL, 1Cu-BGN, 2Cu-BGN, and 5Cu-BGN coatings were imaged by SEM (figure 2). It was observed that Cu-BGNs were randomly scattered (figures 2(b)–(d)), and the density of the scattered Cu-BGNs was higher with more Cu-BGNs incorporated in the coatings. The thickness of the coating was measured to be 8 ± 2 μm.

Coating weight and wettability variations of Cu-BGN coatings are shown in figure 3. The weight gain of Cu-BGN coatings increased steadily with increasing Cu-BGN concentration. In contrast, the water contact angle of PCL and Cu-BGN coatings decreased gradually from around 73 degrees to 63 degrees. Commonly, the smaller the contact angle is, the better the hydrophilicity will be, which favors cell adhesion. Therefore, the results of decreased contact angles of Cu-BGN coatings could be indicative that the biocompatibility of magnesium-based biomaterials is improved by Cu-BGN/PCL composite coatings.

The compositions of freshly prepared samples were analyzed by FTIR spectroscopy, and the results are displayed in figure 4. No obvious peaks are present in the pure Mg curve as no special treatments were applied. The detailed analysis for PCL peaks can be found elsewhere [11]. Besides the peaks of PCL in the Cu-BGN coatings, the peaks at 475 cm^{-1} and 800 cm^{-1} are characteristic bands of Si–O–Si in vibration mode and Si–O in symmetric stretch mode, respectively, belonging to Cu-BGNs [16, 24, 25].

3.2. Electrochemical properties of novel coatings

Electrochemical impedance spectroscopy and potentiodynamic polarization measurements were used to reveal the corrosion protection properties of composite coatings on magnesium in DMEM.

Nyquist plots of pure magnesium and Cu-BGN coatings are displayed in figure 5(a). The plot of pure magnesium showed one capacitive loop at high frequencies (HFs) and one inductive loop at low frequencies (LFs). In comparison to pure magnesium, the inductive loop of Cu-BGN coatings at LFs nearly vanished, and the Nyquist diagram of Cu-BGN coatings is characteristic of two capacitive loops at HFs and LFs. Generally, the capacitive arcs could result from charge transfer and film effects as well as from mass transport

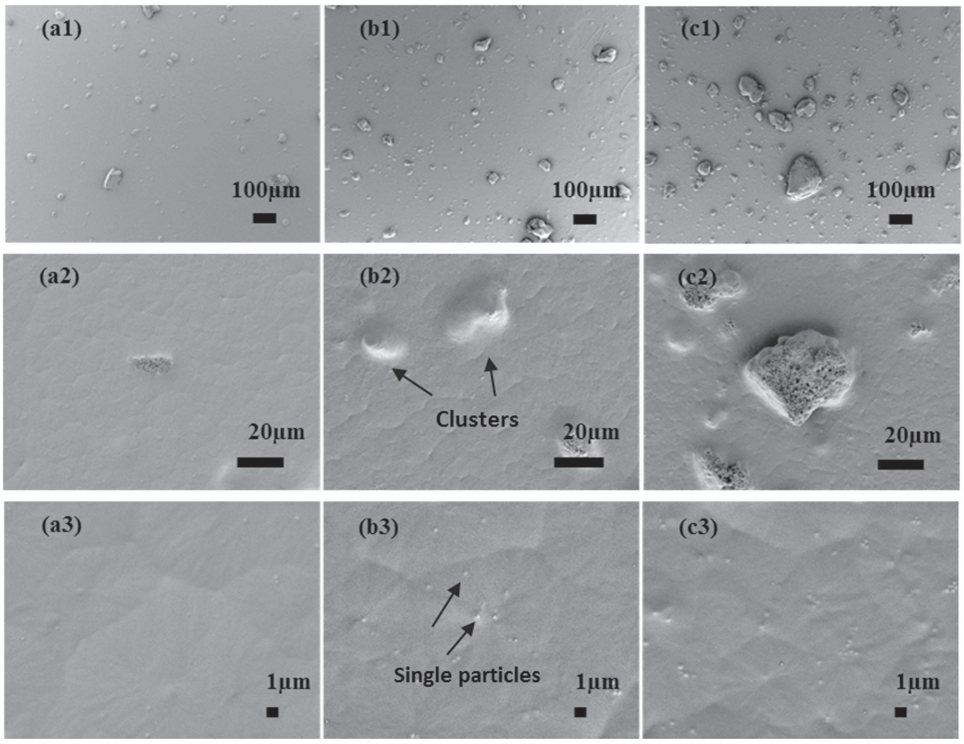

Figure 1. SEM images of 1Cu-BGN(a1–a3), 2Cu-BGN(b1–b3), and 5Cu-BGN(c1–c3) coatings at different magnifications.

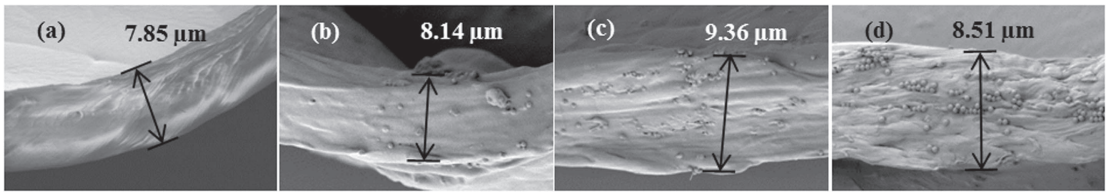

Figure 2. Cross-sectional morphology of pure PCL coating (a), 1Cu-BGN (b), 2Cu-BGN(c), and 5Cu-BGN(d) composite coating.

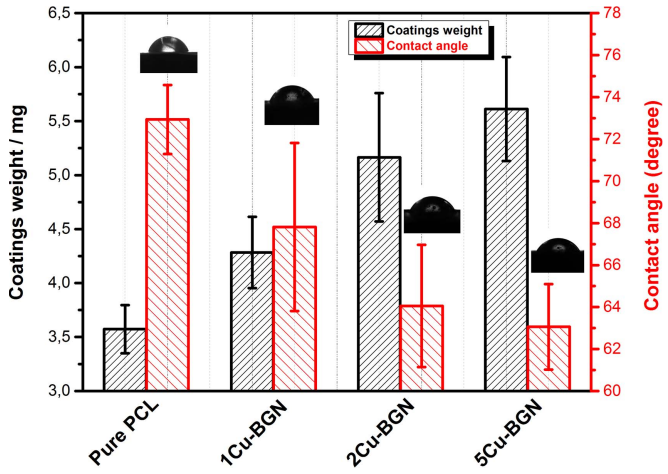

Figure 3. Weight and water contact angle of pure PCL and Cu-BGN coatings.

[26]. The diameter of the capacitive arc is associated with the charge transfer resistance and subsequently with the corrosion resistance. Therefore, the larger diameter of the loop denotes a better corrosion resistance of the sample. The disappearance of the inductive loop suggests a strengthened barrier effect [27].

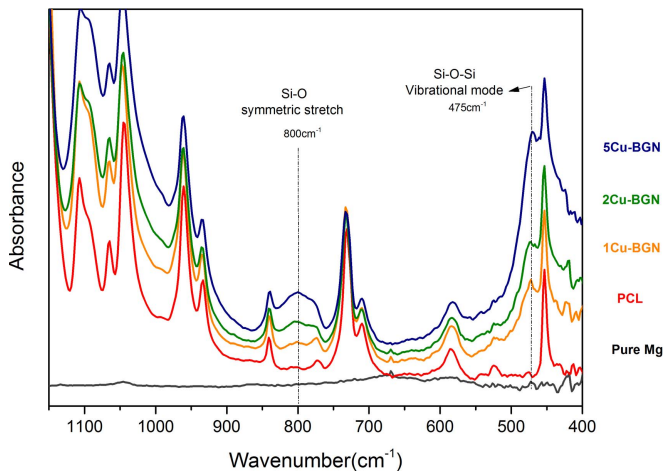

Figure 4. FTIR spectra of pure Mg, PCL, and Cu-BGN coatings.

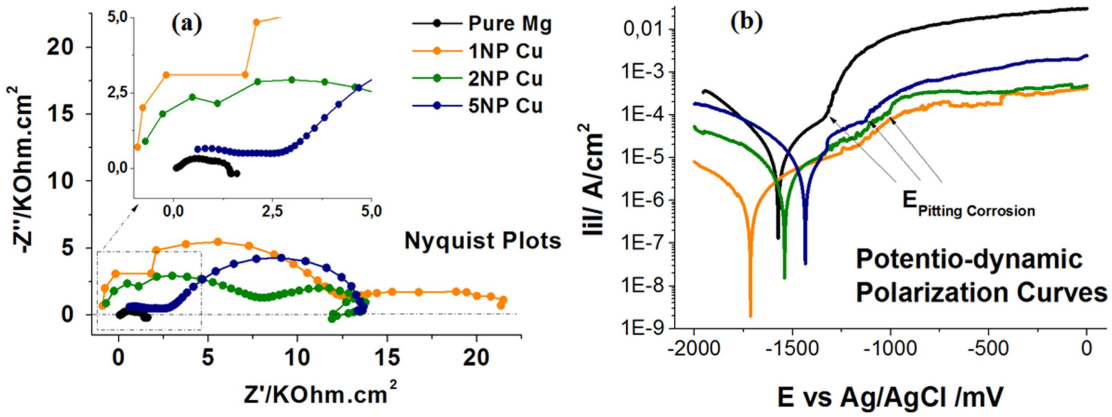

Figure 5. Electrochemical behavior of composite coatings: Nyquist plots (a) and potentiodynamic polarization curves (b).

The anodic and cathodic potentiodynamic polarization curves were collected after impedance measurements in DMEM (shown in figure 5(b)). It demonstrates that increasing Cu-BGN concentration in composite coatings enables the corrosion potential (E_{corr}) in the positive in polarization curves. Furthermore, when comparing the corrosion current density (i_{corr}) of pure magnesium with that of Cu-BGN coatings, i_{corr} of 1Cu-BGN is one order of magnitude lower than the others, and i_{corr} values of 2Cu-BGN and 5Cu-BGN are slightly lower than that of pure magnesium. However, the potential of two coatings is more positive than that of untreated magnesium. Besides, the anodic polarization branch could be ranked as an increasing potential in series: pure Mg > 5Cu-BGN > 2Cu-BGN > 1Cu-BGN. Pitting corrosion occurred for Mg, 5Cu-BGN, and 2Cu-BGN in the anodic branch with increasing applied anodic potential and the breakdown potential (E_{BD}) was reached for Mg, 5Cu-BGN, and 2Cu-BGN at −1.33 V, −1.14 V, and −1.01 V, respectively. The 1Cu-BGN coating shows no clear breakdown potential occurring during anodic polarization, indicating the best corrosion protection for the matrix among all of the coatings. The polarization results are in good agreement with the impedance data. Thereby, the incorporation of Cu-BGNs in PCL coatings improved the corrosion behavior of magnesium, while a higher concentration of Cu-BGNs decreased the anticorrosion properties of the coatings. Nevertheless, even 5Cu-BGN, with the highest concentration of Cu-BGNs in the coatings, exhibited better anticorrosion performance than pure Mg, suggesting the potential of composite coatings for the protection of Mg-based biomedical implants.

3.3. Immersion testing in DMEM

The immersion tests were carried out in DMEM at 37 °C for 7 days. SEM and digital images of pure magnesium, 1Cu-BGN, 2Cu-BGN, and 5Cu-BGN samples were taken to investigate the morphological characteristics after 7 days of immersion.

Typical morphologies (SEM images) are displayed in figure 6 along with optical images (in the bottom-left corner) for samples after 7 days of immersion in

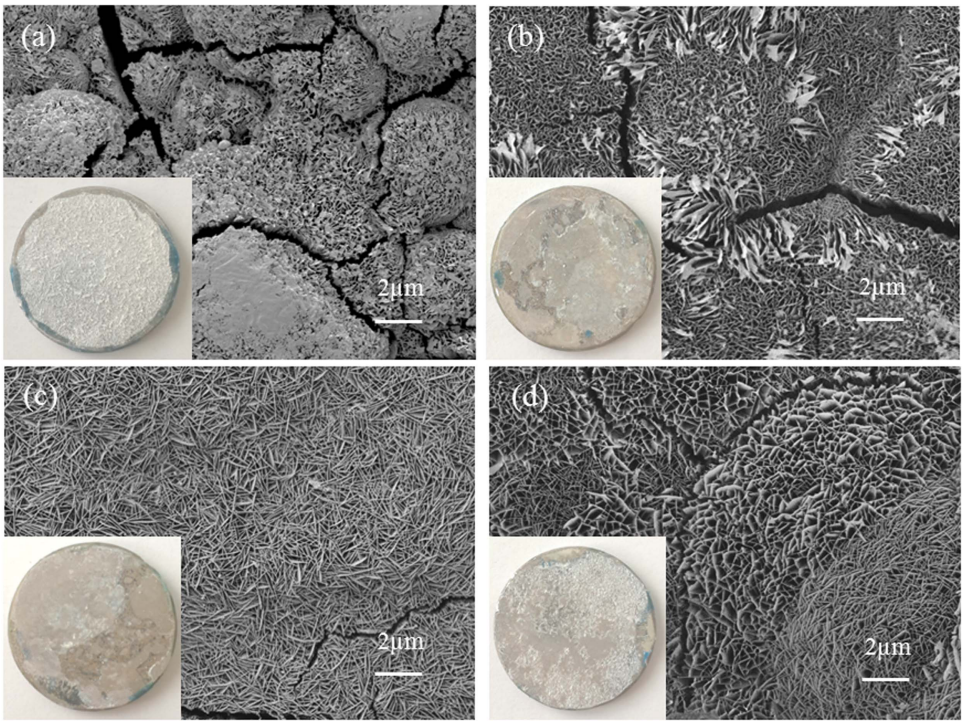

Figure 6. Morphology of pure magnesium (a), 1Cu-BGN (b), 2Cu-BGN (c), and 5Cu-BG (d) samples after 7 days of immersion in DMEM at 37 °C.

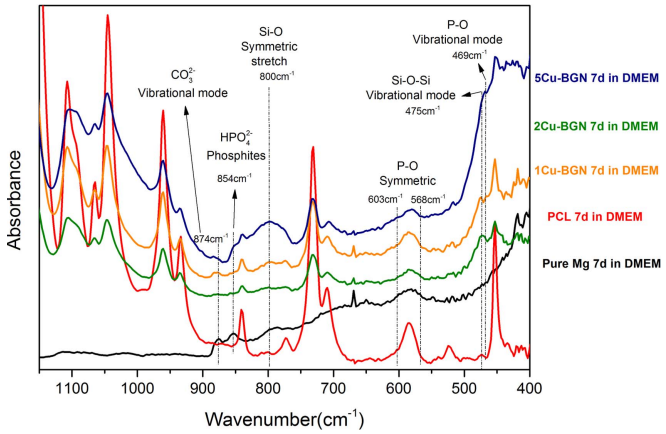

Figure 7. FTIR spectra of pure Mg, PCL, and Cu-BGN coatings immersed in DMEM for 7 days.

DMEM at 37 °C. As shown in the optical images in figure 6(a), whitish loose corrosion products formed on pure magnesium after 7 days of immersion in DMEM. The micro-morphology of pure magnesium after 7 days of soaking is presented in figure 6(a), showing that minor cracks were distributed over the entire surface. As a comparison to the optical images, the Cu-BGN coatings were still visible on the surface, and corrosion products were partially generated on the surface.

This result indicates that samples were well protected by Cu-BGN coatings after 7 days of immersion in DMEM in comparison to the pure Mg samples which showed significant corrosion. With closer observation of SEM images (figures 6(b)–(d)), the formation of characteristically flaked species can be detected on Cu-BGN coatings. Moreover, with increasing Cu-BGN content, more corrosion products were formed.

The chemical composition of the corrosion products from pure magnesium, PCL, and Cu-BGN coatings after 7 days of immersion in DMEM was studied by FTIR spectroscopy and the results are displayed in figure 7.

The bands of Si–O–Si in vibration mode at 475 cm^{-1} and Si–O in symmetric stretch mode at 800 cm^{-1} in Cu-BGN coatings are observed, indicating that Cu-BGNs were still present in the coatings

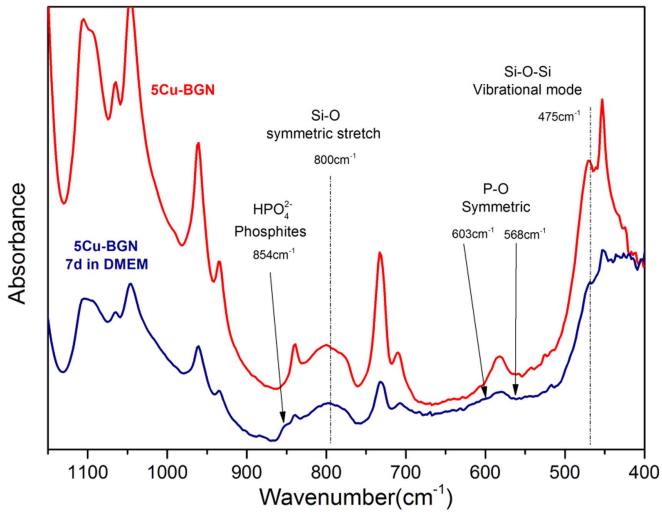

Figure 8. FTIR spectra for 5Cu-BGN before (red) and after (blue) the immersion tests.

after 7 days of immersion in DMEM. It is expected that BG suffers a rapid degradation when in contact with DMEM, which leads to the formation of Ca–P species on the surface [28, 29]. The slow degradation of PCL prevents the buried Cu-BGNs from contacting DMEM, avoiding the risk of being rapidly dissolved in the surrounding medium. Besides the bands at 469 cm^{-1}, 854 cm^{-1}, and 874 cm^{-1} assigned to the P–O vibrational mode, HPO_4^{2-} and CO_3^{2-} corresponding to phosphates and carbonates, respectively, could be found in the spectra of Cu-BGN coatings after 7 days of soaking in DMEM [30–32]. Further, two peaks at 568 cm^{-1} and 603 cm^{-1} are assigned to the symmetric mode of P–O corresponding to phosphate [33]. When making the comparison between 5Cu-BGNs and other Cu-BGNs, it was observed that the relative intensity of the peak at 854 cm^{-1} from 5Cu-BGNs is higher than that of other peaks. It can be concluded that higher content of Cu-BGNs may facilitate the formation of calcium phosphate. Furthermore, two peaks at 854 cm^{-1} and 874 cm^{-1} were also found, which indicates the formation of phosphates and carbonates on pure magnesium after 7 days of immersion in DMEM. The subsequent XPS results were considered to further verify this finding.

To better understand the changes of the immersed samples, the FTIR spectra of 5Cu-BGNs are plotted before (red) and after (blue) 7 days of immersion in DMEM (figure 8). First of all, the intensity of peaks assigned to both PCL and Cu-BGNs after immersion tests decreases, such as the corresponding peaks at 475 cm^{-1} and 800 cm^{-1}. The decrease in intensity of the Si–O or Si–O–Si bands of Cu-BGNs may be due to the degradation of exposed Cu-BGNs during the immersion period. The observation of new peaks at 854 cm^{-1}, 603 cm^{-1}, and 568 cm^{-1} indicates the formation of phosphates on the samples. Therefore, it is confirmed by FTIR that the addition of Cu-BGNs could induce the formation of calcium phosphates on the surface of PCL coatings on magnesium.

The chemical composition of pure magnesium and Cu-BGN coatings after 7 days of immersion in DMEM was also ascertained by XPS characterization. Figure 9 shows the respective C 1s, Mg 2s, O 1s, Ca 2p, and P 2p core-level spectra of the pure magnesium and Cu-BGN coatings after 7 days of immersion in DMEM. The curve-fitted C 1s core-level spectra consisted of three peak components with binding energies at 284.7 eV, 287.3 eV, and 289.6 eV, which are attributed to C=H, C=O, and COOH groups [34]. The XPS spectra of Mg 2s primarily exhibited one main component: MgO (at 89 ± 0.1 eV) and perhaps some $MgCO_3$ present on the top surface [35]. The O 1s core-level spectrum was dominated by the peak component with binding energy at approximately 351.8 eV, which is attributed to the oxidized species [35]. The Ca 2p peaks of the coating are located at 351.1 eV (±0.1 eV) (2p1/2) corresponding to calcium phosphate [36]. The original P 2p spectrum can be de-convoluted into two peaks of C–P–O at 134.9 eV and P–O at 132.7 eV, according to the literature [37]. The XPS results show that the corrosion products of Cu-BGN coatings after 7 days of immersion were mainly composed of magnesium oxide, magnesium phosphate, calcium phosphate, and perhaps a small amount of magnesium carbonate or calcium carbonate.

3.4. Antibacterial activity tests

The correlation between antibacterial activity and Cu^{2+} ion release from different Cu-BGN coatings was investigated and results are shown in figure 10. Optical density ($OD600_{nm}$) of bacteria co-cultured with extracts from coatings in PBS (72 h immersion) was measured to evaluate the antibacterial activity of Cu-BGN coatings. The higher OD value is related to the increased turbidity of the suspension, which results from bacteria growth during the incubation process.

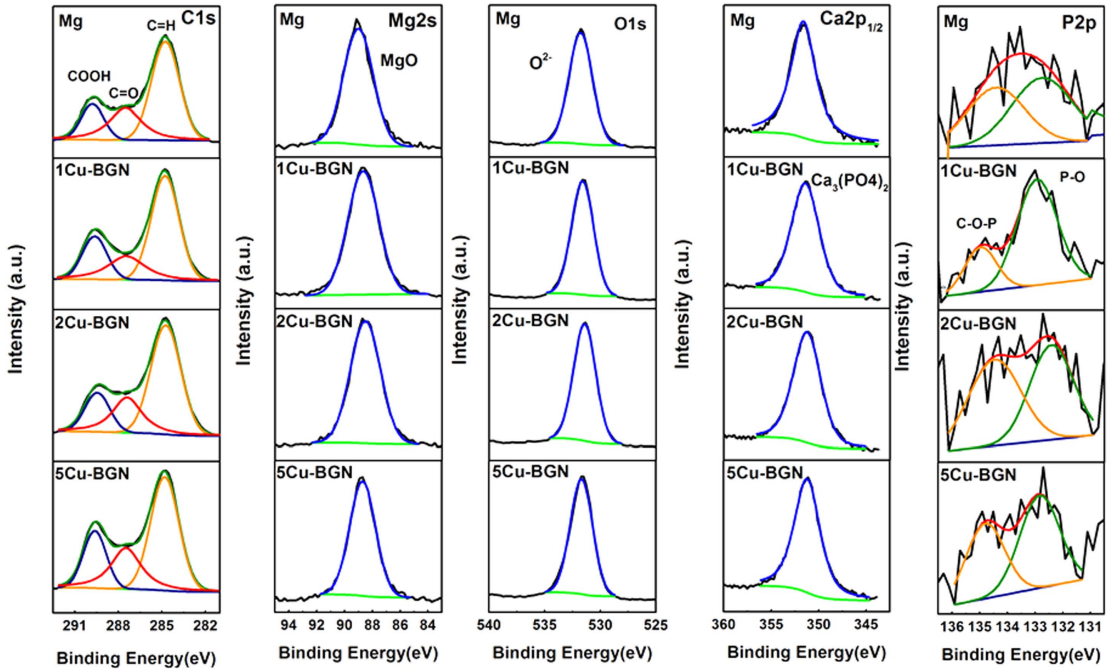

Figure 9. XPS high-resolution spectra of C 1s, Mg 2s, O 1s, Ca 2p, and P 2p detected on pure magnesium, 1Cu-BGN, 2Cu-BGN, and 5Cu-BGN after 7 days of immersion in DMEM.

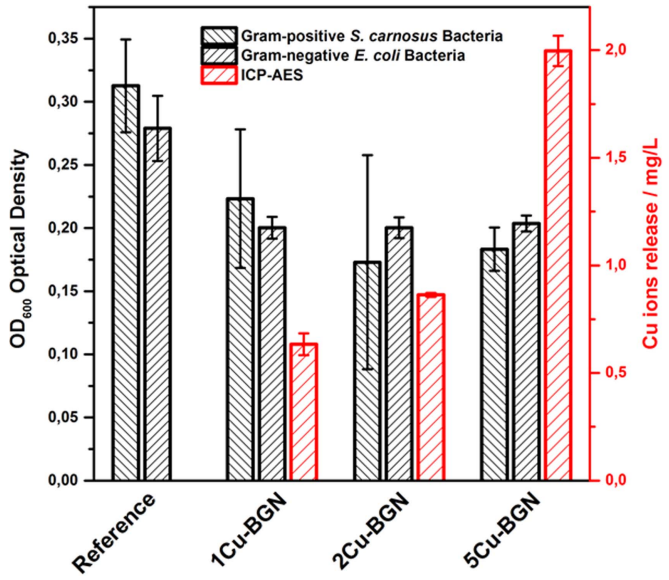

Figure 10. Optical density of bacteria co-cultured with coating extract after 24 h in PBS and release of Cu^{2+} ions from Cu-BGN coating after 72 h in PBS.

The OD_{600nm} values of Cu-BGN coatings decreased in both bacteria types compared to the reference values. The results indicate that the bacterial activity of *S. carnosus and E. coli* was inhibited when the Cu-BGN extracts were added to the medium.

The Cu^{2+} ion release levels increased with an increasing content of Cu-BGNs in PCL coatings, from 0.63 mg l^{-1}, 0.86 mg l^{-1}, and 1.99 mg l^{-1} for 1Cu-BGN, 2Cu-BGN, and 5Cu-BGN, respectively. The increased Cu^{2+} ion levels with increasing Cu-BGN incorporation led to an approximate 20% decrease in bacterial activity in the culture medium, but this did not increase further at higher Cu release (figure 10). For example, there is no further drop of OD value for 5Cu-BGN compared to 2Cu-BGN, where the Cu^{2+} ion release level is even 1 mg l^{-1} lower than in 5Cu-BGN. This phenomenon is likely due to the concentration of Cu^{2+} ions in this range exhibiting a similar bacterial inhibition effect. Nevertheless, the decreased OD values of Cu-BGN coatings compared to the reference demonstrated growth restriction of *S. carnosus* and *E. coli* by the released Cu^{2+} ions.

3.5. Cyto-compatibility assessment

The cyto-compatibility of biomaterials is another important aspect that needs to be investigated for biomedical applications. Although the released Cu^{2+} ions from the composite coatings could inhibit bacteria growth, the ions may impose adverse effects on cell adhesion and proliferation. Therefore, both cytotoxicity and cell contact assays were carried out to study the cyto-compatibility of PCL/Cu-BGN coated magnesium substrates. Cell adhesion and proliferation were systematically investigated, using the direct contact assay. The indirect (cytotoxicity) assay mainly aims to assess the influence of released Cu^{2+} ions from coatings on the activity of MG-63 cells.

3.5.1. Direct assessment

Biomineralization structures were assessed by fluorescent staining of calcium phosphate with a commercial mineralization kit (OsteoImage). The intensity of the green fluorescence is proportional to the amount of calcium phosphate formed on the surface of the sample. The fluorescence images indicating mineralization of pure Mg, 1Cu-BGN, 2Cu-BGN, 5Cu-BGN, and the control group after 72 h of cultivation with MG-63 cells are displayed in figures 11(a), (c), (e), (g), (i). As the fluorescence image in figure 11(a) shows, a large proportion of calcium phosphate/magnesium phosphate (confirmed by FTIR and XPS) formed on the surface of pure magnesium after 3 days of cultivation with MG-63 cells. Due to the release of Mg^{2+} ions, hydrogen bubbles, and alkalization of the solution by the OH^{-} ions, the formed corrosion products would barely cling to the matrix and finally they peeled off from the surface and diffused into the medium, whereas the mineralization on Cu-BGN/PCL coatings was locally scattered over the entire surface of Cu-BGNs in PCL coatings (figure 1). The proportion and intensity of calcium phosphate formation shown in figures 11(c), (e), (g) are related to the relatively high content of Cu-BGNs in these coatings. It indicates that increasing contents of Cu-BGNs enhances the bioactivity of the coating system.

To visualize cell morphology and cell distribution on composite coatings, MG-63 cells were labeled with Vybrant™ Dil in a cell-labeling solution. Dil is a lipophilic tracer useful for labeling the membranes of living cells. The fluorescence images of Dil labeled MG-63 cells on pure Mg, 1Cu-BGN, 2Cu-BGN, 5Cu-BGN, and control group are shown in figures 11(b), (d), (f), (h), (j) at the same spot where images by OsteoImage were observed. Fewer living cells are seen to adhere to pure magnesium surfaces (figure 11(b)). The cell density of Cu-BGN coatings was greater than that of pure magnesium after 72 h of culture, which indicates improved cell adhesion and proliferation by Cu-BGN coatings. MG-63 cells show homogenous membrane spreading on Cu-BGN coatings on magnesium substrates, indicating the favorable surface characteristics offered by the Cu-BGN coated substrates. For a closer observation, cell morphology and attachment to 1Cu-BGN coating and to the control group showed no visible qualitative differences. It was also observed that the expressed cell phenotype on Cu-BGN coatings and on the control group was similar to each other. Besides, the cell density of Cu-BGN coatings slightly decreased as more Cu-BGNs were added. The slightly decreased cell density might be caused by the rougher and less regular surface (seen in figure 1), which has a negative effect on cell adhesion and proliferation on coated samples [38]. For example, the cell attachment can be affected by the prominent Cu-BGN clusters, which increase the roughness of the coatings. Cells can barely adhere on or around the clusters, but they attach on the smooth area on the coatings. Therefore, the increasing number of clusters in the coatings finally may lead to the slightly reduced cell adhesion as observed in figures 11(d), (f), (h).

Relative cell viability, LDH activity, and ALP activity of the adherent MG-63 cells on pure magnesium and Cu-BGN coatings are shown in figures 12(a)–(c). The results of the WST-8 assay in all Cu-BGN coatings showed significantly higher viability in comparison to the pure magnesium after 72 h of culture, which reflects a larger number of viable cells adhering to Cu-BGN coatings over time. The relative cell viability of Cu-BGN coatings exhibited a slight gradual downward trend at higher Cu-BGN content. Among all Cu-BGN coatings, the MG-63 cells' relative viability on the 1Cu-BGN coating was the highest, with a value of 76.7% compared to the control. The decreased cell viability was probably caused by the rougher surface morphology due to larger amounts of Cu-BGNs incorporated in the coating, as shown in figures 1 and 2. The dissolution of Cu-BGNs in PCL coatings during cultivation may also influence the cell adhesion. These factors may play a negative role in cell adhesion and proliferation as the extracts in indirect tests have no adverse effect on cell activity. On the contrary, the extract of 5Cu-BGN showed MG-63 cells with the highest viability (in figure 13(f)) among all samples.

LDH activity closely correlates with the metabolic activity of cells, which has also been used in preclinical investigations to test the biocompatibility of materials [39]. Like the results from the WST-8 assay, similar results were observed from LDH activity tests, as shown in figure 12(b), where MG-63 cells grown on pure magnesium showed rather low LDH activity compared to that of Cu-BGN coatings after 72 h of cultivation. A decreasing trend in LDH activity was detected with increasing Cu-BGN content. According to the literature [40], a linear relationship exists between cell concentration and LDH activity, which could be used to investigate mammalian cell proliferation behavior. Although the LDH assay was not employed to determine cell numbers in the present research, the comparative view of cell proliferation could be evaluated from the LDH activity results in figure 12(b) and from fluorescent images with Vybrant

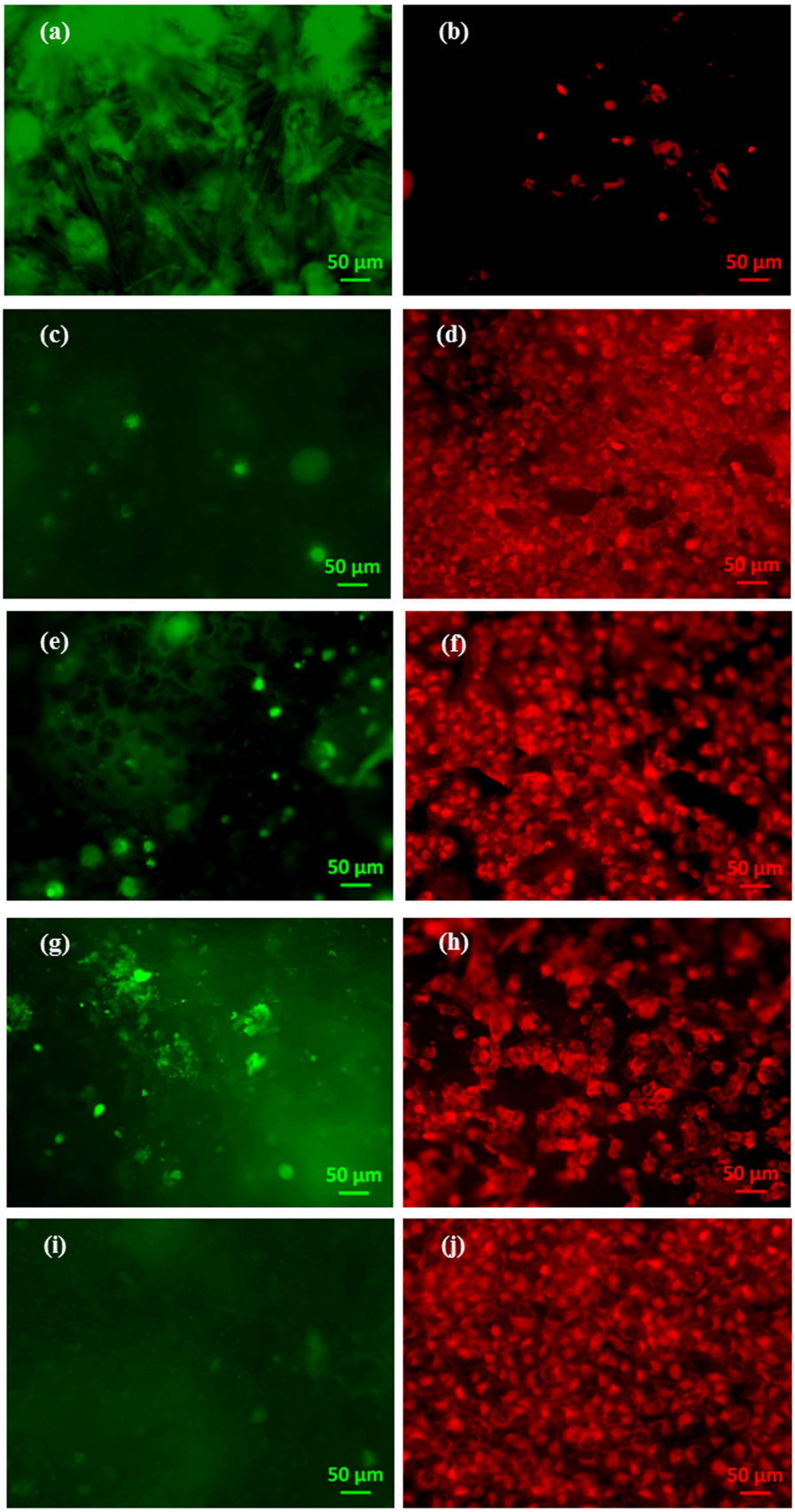

Figure 11. Fluorescence imaging and osteoblast mineralization assessment using OsteoImage illustrating pure Mg(a), 1Cu-BGN(c), 2Cu-BGN(e), and 5Cu-BGN(g) co-cultured with MG-63 cells in DMEM after 72 h and control groups (i). Vybrant®Dil stained MG-63 cells seeded on pure Mg(b), 1Cu-BGN(d), 2Cu-BGN(f), 5Cu-BGN(h), and control group after 72 h of cultivation. Both OsteoImage (green, left) and Vybrant Dil (red, right) were fluorescently imaged at the same spot for each sample.

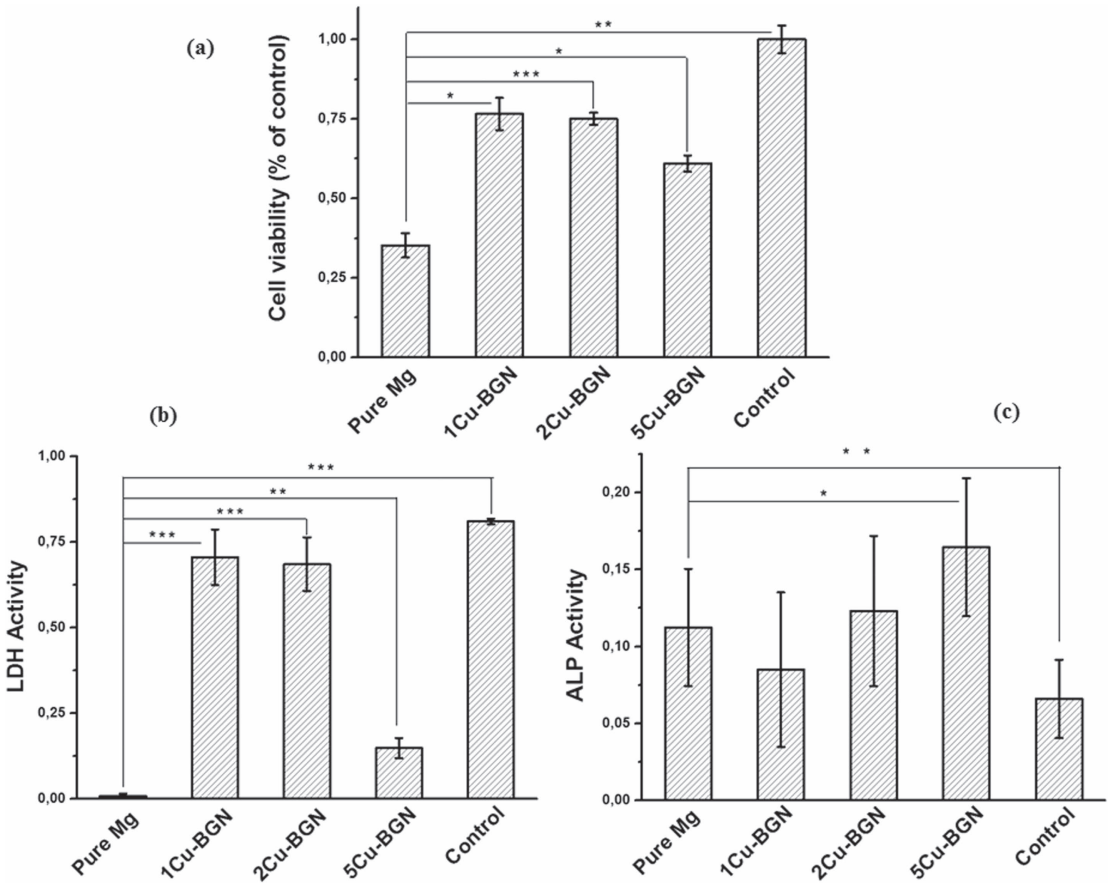

Figure 12. Relative cell viability on pure magnesium and Cu-BGN coatings as detected by the WST-8 assay in direct contact testing after 72 h co-cultivation with MG-63 cells (a). The data were normalized to positive control values (DMEM only, without any sample), which was set at 100% cell viability. LDH (b) and ALP activities (c) of MG-63 cells on pure magnesium and Cu-BGN coatings in DMEM after 72 h of co-cultivation. Pure magnesium was used as the reference in WST-8, LDH, and ALP assays. Asterisks denote significant differences compared to pure magnesium, $^{*}p < 0.05$, $^{**}p < 0.01$ and $^{***}p < 0.001$.

Dil in figure 11. The LDH activity value of MG-63 cells on Cu-BGN coatings was much higher than that on pure magnesium. Even the lowest activity value from 5Cu-BGN coating was still much higher than from the control group. Therefore, all Cu-BGN coatings highly promoted cell proliferation and cell activity. The increased addition of Cu-BGNs led to a slight downward trend in cell proliferation and cell activity. The control group showed the highest LDH activity compared with other groups. The results of WST-8 assay and LDH test are in good agreement with the fluorescent images stained with Vybrant Dil shown in figure 11.

ALP is expressed very early during the biomineralization process and early during osteoblastogenesis and is continuously associated with the region of highest ossification [41]. It is easier to understand the ALP results in figure 12(c) by combining them with the OsteoImage fluorescent images in figure 11. The larger proportion of the green area in the fluorescent images represents more calcium phosphate accumulation, which indicates higher ALP activity. Therefore, ALP activity of MG-63 cells on pure magnesium was higher than 1Cu-BGN and 2Cu-BGN, which could also be observed in the fluorescent images. The cell ALP activity on 5Cu-BGN possesses the highest value as compared with the other samples in figure 12(c). The highest intensity of localized green color from the 5Cu-BGN fluorescent image indicated a large proportional amount of calcium phosphate. This could be the reason why the ALP activity of MG-63 cells on 5Cu-BGN was the highest. ALP activity of the control group was found to be the lowest among all samples, and that there is less green area displayed in figure 11(i) is in agreement with the ALP activity results.

3.5.2. Indirect assays

The viability and morphology of living cells were assessed by using Calcein-AM and WST-8 assay, respectively. Calcein-AM stains the cytoplasm of living cells and gives information about the plasma membrane integrity and intracellular esterase activity, which are the hallmarks of the normal cells in equilibrium [42]. Live cells fluorescently green-stained are shown in figures 13(a)–(d), which are assigned to MG-63 cells co-cultured with extracts from pure magnesium, 1Cu-BGN, 2Cu-BGN, and 5Cu-BGN for 72 h of immersion in DMEM. Figure 13(e) was taken as a positive control. The cell density on Cu-BGN coatings was almost as high as the positive control,

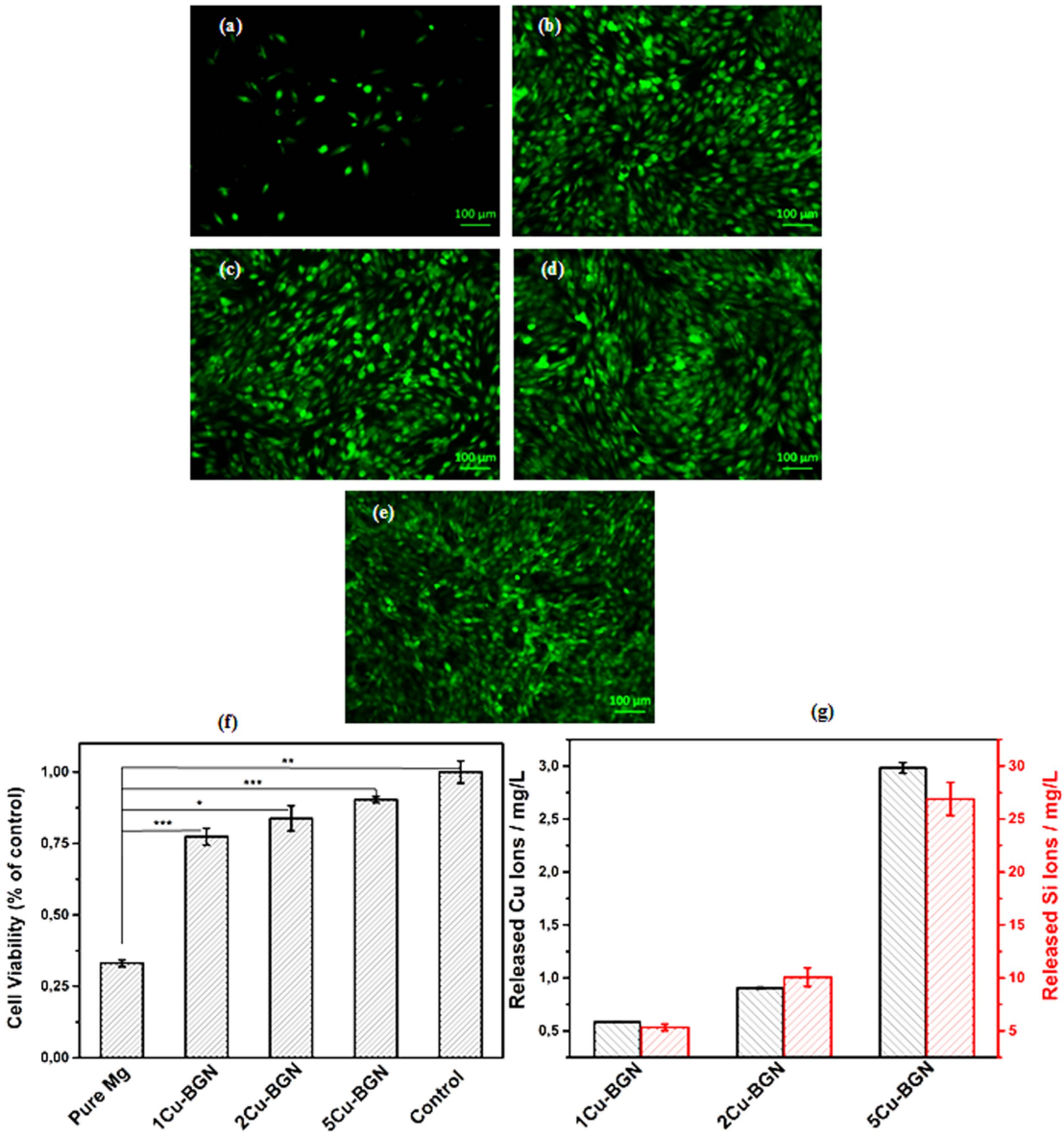

Figure 13. Live-stained MG63 cells with Calcein-AM (green) at 48 h cultivation with the extracts of pure Mg samples (a), 1Cu-BGN (b), 2Cu-BGN (c), and 5Cu-BGN (d), which were immersed for 72 h in DMEM and the control group (e), and relative cell viability in WST-8 assay compared to control (f). Pure magnesium was used as the reference for each assay. Asterisks denote significant differences compared to pure magnesium, $^{*}p < 0.05$, $^{**}p < 0.01$ and $^{***}p < 0.001$. Copper and silicon ions released in extracts from Cu-BGN coatings after 72 h incubation in DMEM (g).

while that of pure Mg was quite low. The cell density results confirmed the favorable medium provided by the extracts from all coatings. Besides, the cell distribution of Cu-BGN coatings displayed a higher uniformity than that of bare magnesium. The results of WST-8 assay in figure 13(f) support the same argument. The relative cell activity of Cu-BGN coatings was above 80%, when taking the positive control as 100%. The relative activity of pure Mg was only 36% compared to the control. Interestingly, with increasing content of Cu-BGNs in PCL coatings, a higher cell activity was measured. In order to explain this phenomenon, the copper and silicon ion release in the extracts of Cu-BGN coatings immersed in DMEM was examined by ICP-AES, and the results are displayed in figure 13(g). The amounts of released Cu^{2+} ions from 1Cu-BGN, 2Cu-BGN, and 5Cu-BGN after 72 h of immersion in DMEM were 0.58 mg l^{-1}, 0.90 mg l^{-1}, and 2.98 mg l^{-1}, respectively. The values for Si release were approximately ten times higher than those of copper ions. Theoretically, the release of calcium ions also occurred during the immersion process. Since the calcium ion concentration released from the Cu-BGN coatings was almost 100 times lower than the calcium ion concentration contained in DMEM, the effect of released calcium ions can be neglected. A recent report indicated that physiological concentrations of soluble Si stimulates collagen type 1 synthesis in human osteoblast-like cells (especially MG-63 cells) and promotes osteoblastic differentiation [43]. The enhanced cell activity with increased amounts of Cu-BNGs in coatings may mainly be due to the relatively

high Si ions concentration in the extracts. Therefore, we can conclude that higher contents of Cu-BGNs in the PCL coatings, at least within the concentrations investigated in this study, have positive consequences on cell viability.

4. Conclusions

A new family of bioactive coatings for Mg based on Cu-BGN/PCL composites has been developed and characterized. Cu-BGNs were randomly scattered in PCL coatings and clusters of different sizes were observed with increasing content of Cu-BGNs. A slightly decreasing water contact angle was measured in the coatings with increasing Cu-BGN content. Electrochemical measurements indicated that the corrosion resistance of magnesium was increased by Cu-BGN incorporation in PCL coatings. The increasing concentration of Cu-BGNs, however, led to a slight decrease of anticorrosion properties. However, the corrosion resistance of all Cu-BGN/PCL coatings was significantly higher than that of pure magnesium. The chemical composition analysis upon 7 days of immersion showed that higher Cu-BGN content in PCL coatings facilitates calcium phosphate formation. The measurement of antibacterial activity indicated that the growth of both *S. carnosus* and *E. coli* was restricted by the release of Cu^{2+} ions from Cu-BGN coatings, however, the increase of Cu^{2+} ion levels in the culture medium showed no significant increased antibacterial effect. Indirect and direct cyto-compatibility experiments indicated that the Cu-BGN coatings could strongly promote the viability and proliferation of MG-63 cells compared to pure magnesium. A slight decrease in cell proliferation and cell activity occurred with increasing Cu-BGN concentration in the coatings, and the rougher surface morphology and higher effect of Cu-BGN dissolution products could be the reason for this effect. This new group of bioactive, antibacterial composite coatings must be now evaluated in long-term *in vitro* experiments to assess the stability of the corrosion protection effect and the maintenance of bioactivity and antibacterial properties.

Acknowledgments

The authors would like to thank Xuemei Zhou (Chair for Surface Science and Corrosion) and Alina Grünewald (Institute of Biomaterials) from University of Erlangen-Nuremberg, Germany, for experimental support. Financial support was provided by the China Scholarship Council (CSC) No. 201308230074 for Yuyun Yang and for W H G by the German Science Foundation (DFG, Go598).

Notes

The authors declare no competing financial interest.

ORCID iDs

Sannakaisa Virtanen https://orcid.org/0000-0002-7179-7593
Aldo R Boccaccini https://orcid.org/0000-0002-7377-2955

References

[1] Hélary G, Noirclère F, Mayingi J and Migonney V 2009 A new approach to graft bioactive polymer on titanium implants: improvement of MG 63 cell differentiation onto this coating *Acta Biomater.* **5** 124–33
[2] Laurencin D *et al* 2011 Magnesium incorporation into hydroxyapatite *Biomaterials* **32** 1826–37
[3] Keim S, Brunner J G, Fabry B and Virtanen S 2011 Control of magnesium corrosion and biocompatibility with biomimetic coatings *J. Biomed. Mater. Res.* B **96** 84–90
[4] Ostrowski N, Lee B, Enick N, Carlson B, Kunjukunju S, Roy A and Kumta P N 2013 Corrosion protection and improved cytocompatibility of biodegradable polymeric layer-by-layer coatings on AZ31 magnesium alloys *Acta Biomater.* **9** 8704–13
[5] Schinhammer M, Steiger P, Moszner F, Löffler J F and Uggowitzer P J 2013 Degradation performance of biodegradable Fe-Mn-C(-Pd) alloys *Mater. Sci. Eng.* C **33** 1882–93
[6] Kraus T, Fischerauer S F, Hänzi A C, Uggowitzer P J, Löffler J F and Weinberg A M 2012 Magnesium alloys for temporary implants in osteosynthesis: *in vivo* studies of their degradation and interaction with bone *Acta Biomater.* **8** 1230–8
[7] Wang H and Shi Z 2011 *In vitro* biodegradation behavior of magnesium and magnesium alloy *J. Biomed. Mater. Res.* B **98** 203–9
[8] Lin X, Tan L, Zhang Q, Yang K, Hu Z, Qiu J and Cai Y 2013 The *in vitro* degradation process and biocompatibility of a ZK60 magnesium alloy with a forsterite-containing micro-arc oxidation coating *Acta Biomater.* **9** 8631–42
[9] Zhao Y, Jamesh M I, Li W K, Wu G, Wang C, Zheng Y, Yeung K W K and Chu P K 2014 Enhanced antimicrobial properties, cytocompatibility, and corrosion resistance of plasma-modified biodegradable magnesium alloys *Acta Biomater.* **10** 544–56
[10] Jin G, Yang Y, Cui X, Liu E, Wang Z and Li Q 2011 Chrome-free neodymium-based protective coatings for magnesium alloys *Mater. Lett.* **65** 1145–7
[11] Yang Y, Michalczyk C, Singer F, Virtanen S and Boccaccini A R 2015 *In vitro* study of polycaprolactone/bioactive glass composite coatings on corrosion and bioactivity of pure Mg *Appl. Surf. Sci.* **355** 832–41
[12] Hornberger H, Virtanen S and Boccaccini A R 2012 Biomedical coatings on magnesium alloys—a review *Acta Biomater.* **8** 2442–55
[13] Griffith L G 2000 Polymeric biomaterials *Acta Mater.* **48** 263–77
[14] Xu L and Yamamoto A 2012 Characteristics and cytocompatibility of biodegradable polymer film on magnesium by spin coating *Colloids Surf.* B **93** 67–74
[15] Zheng K, Lu M, Rutkowski B, Dai X, Yang Y, Taccardi N, Stachewicz U, Czyrska-Filemonowicz A, Hüser N and Boccaccini A R 2016 ZnO quantum dots modified bioactive glass nanoparticles with pH-sensitive release of Zn ions, fluorescence, antibacterial and osteogenic properties *J. Mater. Chem.* B 7936–49
[16] Saboori A, Rabiee M, Moztarzadeh F, Sheikhi M, Tahriri M and Karimi M 2009 Synthesis, characterization and *in vitro* bioactivity of sol-gel-derived SiO_2-CaO-P_2O_5-MgO bioglass *Mater. Sci. Eng.* C **29** 335–40
[17] Brunner T J, Grass R N and Stark W J 2006 Glass and bioglass nanopowders by flame synthesis *Chem. Commun.* **17** 1384–6
[18] Wu C, Zhou Y, Xu M, Han P, Chen L, Chang J and Xiao Y 2013 Copper-containing mesoporous bioactive glass scaffolds with multifunctional properties of angiogenesis capacity, osteostimulation and antibacterial activity *Biomaterials* **34** 422–33

[19] Balamurugan A, Balossier G, Laurent-Maquin D, Pina S, Rebelo A H S, Faure J and Ferreira J M F 2008 An *in vitro* biological and anti-bacterial study on a sol–gel derived silver-incorporated bioglass system *Dent. Mater.* **24** 1343–51
[20] Kozon D, Zheng K, Boccardi E, Liu Y, Liverani L and Boccaccini A R 2016 Synthesis of monodispersed Ag-doped bioactive glass nanoparticles via surface modification *Materials* **9** 225–33
[21] Ericksen B, Wu Z, Lu W and Lehrer R I 2005 Antibacterial activity and specificity of the six human {alpha}-defensins *Antimicrob. Agents Chemother.* **49** 269–75
[22] Amin R, Krammer B, Abdel-Kader N, Verwanger T and El-Ansary A 2010 Antibacterial effect of some benzopyrone derivatives *Eur. J. Med. Chem.* **45** 372–8
[23] ISO 10993–5 2009 Biological Evaluation of Medical Devices—Part 5: Tests for *In Vitro* Cytotoxicity (International Organization for Standardization)
[24] El-Kady A M, Rizk R A, Abd El-Hady B M, Shafaa M W and Ahmed M M 2012 Characterization, and antibacterial properties of novel silver releasing nanocomposite scaffolds fabricated by the gas foaming/salt-leaching technique *J. Genet. Eng. Biotechnol.* **10** 229–38
[25] Chen Q, Yang Y, Pérez de Larraya U, Garmendia N, Virtanen S and Boccaccini A R 2016 Electrophoretic co-deposition of cellulose nanocrystals-45S5 bioactive glass nanocomposite coatings on stainless steel *Appl. Surf. Sci.* **362** 323–8
[26] Xin Y, Huo K, Tao H, Tang G and Chu P K 2008 Influence of aggressive ions on the degradation behavior of biomedical magnesium alloy in physiological environment *Acta Biomater.* **4** 2008–15
[27] Wang Y, Wang W, Zhong L, Wang J, Jiang Q and Guo X 2010 Super-hydrophobic surface on pure magnesium substrate by wet chemical method *Appl. Surf. Sci.* **256** 3837–40
[28] Sepulveda P, Jones J R and Hench L L 2002 Bioactive sol-gel foams for tissue repair *J. Biomed. Mater. Res.* **59** 340–8
[29] Sepulveda P, Jones J R and Hench L L 2002 *In vitro* dissolution of melt-derived 45S5 and sol-gel derived 58 s bioactive glasses *J. Biomed. Mater. Res.* **61** 301–11
[30] Tan Q, Ji J, Barbosa M A, Fonseca C and Shen J 2003 Constructing thromboresistant surface on biomedical stainless steel via layer-by-layer deposition anticoagulant *Biomaterials* **24** 4699–705
[31] Wang J, de Groot K, van Blitterswijk C and de Boer J 2009 Electrolytic deposition of lithium into calcium phosphate coatings *Dent. Mater.* **25** 353–9
[32] Rehman I and Bonfield W 1997 Characterization of hydroxyapatite and carbonated apatite by photo acoustic FTIR spectroscopy *J. Mater. Sci., Mater. Med.* **8** 1–4
[33] Ma J, Chen C Z, Wang D G, Meng X G and Shi J Z 2010 Influence of the sintering temperature on the structural feature and bioactivity of sol-gel derived SiO_2-CaO-P_2O_5 bioglass *Ceram. Int.* **36** 1911–6
[34] Moulder J F, Stickle W F, Sobol P E, Bomben K D and Bomden K D 1995 *Handbook of X-Ray Photoelectron Spectroscopy* (Eden Prairie, MN: Perkin-Elmer) pp 255
[35] Luo Y, Wang X, Guo W and Rohwerder M 2015 Growth behavior of initial product layer formed on Mg alloy surface induced by polyaniline *J. Electrochem. Soc.* **162** C294–301
[36] Chusuei C C, Goodman D W, Van Stipdonk M J, Justes D R and Schweikert E A 1999 Calcium phosphate phase identification using XPS and time-of-flight cluster SIMS *Anal. Chem.* **71** 149–53
[37] Azuma H 1992 Negative electrode material, manufacturing thereof, and nonaqueous electrolyte battery made therefrom *Patent* WO 92/16026 (17.09.92 92/24)
[38] Anselme K, Bigerelle M, Noel B, Dufresne E, Judas D, Iost A and Hardouin P 2000 Qualitative and quantitative study of human osteoblast adhesion on materials with various surface roughnesses *J. Biomed. Mater. Res.* **49** 155–66
[39] Chiappini C, De Rosa E, Martinez J O, Liu X, Steele J, Stevens M M and Tasciotti E 2015 Biodegradable silicon nanoneedles delivering nucleic acids intracellularly induce localized *in vivo* neovascularization *Nat. Mater.* **14** 532–9
[40] Allen M, Millett P, Dawes E and Rushton N 1994 Lactate dehydrogenase activity as a rapid and sensitive test for the quantification of cell numbers *in vitro Clin. Mater.* **16** 189–94
[41] Sarker B, Papageorgiou D G, Silva R, Zehnder T, Gul-E-Noor F, Bertmer M, Kaschta J, Chrissafis K, Detsch R and Boccaccini A R 2014 Fabrication of alginate–gelatin crosslinked hydrogel microcapsules and evaluation of the microstructure and physico-chemical properties *J. Mater. Chem.* B **2** 1470
[42] Joshi C, Karumuri B, Newman J J and Decoster M A 2012 Cell morphological changes combined with biochemical assays for assessment of apoptosis and apoptosis reversal *Current Microscopy Contributions to Advances in Science and Technology* ed A Méndez-Vilas (Badajoz: Formatex) pp 756–62
[43] Reffitt D, Ogston N, Jugdaohsingh R, Cheung H F, Evans B A, Thompson R P, Powell J and Hampson G 2003 Orthosilicic acid stimulates collagen type 1 synthesis and osteoblastic differentiation in human osteoblast-like cells *in vitro Bone* **32** 127–35